Journal of Marine Science and Technology
https://doi.org/10.1007/s00773-024-00988-3

ORIGINAL ARTICLE

Basic design optimization of power and desalinated water for hybrid cycle ocean thermal energy conversion system integrated with desalination plant

Ahmad Aiman Azmi[1,2,3] · Takeshi Yasunaga[2] · Kevin Fontaine[2] · Takafumi Morisaki[2] · Tsutomu Nakaoka[2] · Sathiabama T. Thirugnana[3] · Abu Bakar Jaafar[3] · Yasuyuki Ikegami[2]

Received: 16 November 2023 / Accepted: 20 January 2024

Abstract

Ocean thermal energy conversion (OTEC) is a heat engine application that utilizes the Rankine cycle to extract energy from the thermal gradient between surface seawater and deep seawater. Hybrid cycle OTEC (H-OTEC) is a combination of an open cycle desalination system and a closed-cycle power generation system that leverages the features of both cycles. Unlike other desalination technologies that require extensive energy to operate, H-OTEC relies entirely on renewable energy. In addition, a desalination plant can be coupled with the H-OTEC system (H-OTEC + D) to improve its performance. Conventionally, the total heat transfer area of heat exchangers per net power is used as an objective function to achieve optimal performance with the lowest capital expenditure cost. The proposed objective function, unlike the conventional one, considers both power and water. In this study, the optimization of H-OTEC + D and H-OTEC is carried out by minimizing the proposed objective function, considering several independent variables. The performance of both systems is evaluated in terms of the objective function, power consumption, seawater flow rates, and desalination ratio. The findings also indicate the effectiveness of the proposed objective function over the conventional one as an effective tool for maximizing power and desalinated water generation.

Keywords Ocean thermal energy conversion · Hybrid cycle · Integrated · Desalination · Renewable energy

List of symbols

Symbols

A	Area (m^2)
C	Clearance (m)
cp	Specific heat capacity (kJ kg^{-1} K^{-1})
D	Diameter (m)
f	Friction factor (–)
g	Gravitational acceleration (m s^{-2})
G	Mass flux (kg s^{-1} m^{-2})
h	Specific enthalpy (kJ kg^{-1})
H	Height (m)
K	Loss of coefficient (–)
L	Specific latent heat (kJ kg^{-1})
L_p	Length of the pipe (m)
m	Mass flow rate (kg s^{-1})

✉ Ahmad Aiman Azmi
ahmadaiman.azmi94@gmail.com

Takeshi Yasunaga
yasunaga@ioes.saga-u.ac.jp

Kevin Fontaine
fontaine.kevin.d@gmail.com

Takafumi Morisaki
morisaki@ioes.saga-u.ac.jp

Tsutomu Nakaoka
nakaoka@ioes.saga-u.ac.jp

Sathiabama T. Thirugnana
sathiabama@utm.my

Abu Bakar Jaafar
bakar.jaafar@utm.my

Yasuyuki Ikegami
ikegami@cc.saga-u.ac.jp

[1] Graduate School of Science and Engineering, Saga University, Saga, Japan

[2] Institute of Ocean Energy Saga University, Saga, Japan

[3] UTM Ocean Thermal Energy Centre, Universiti Teknologi Malaysia, Kuala Lumpur, Malaysia

Published online: 08 February 2024

N	Number of plates (–)
P	Pressure
Pr	Prandtl number (–)
Q	Heat flow rate (kJ)
Re	Reynold number (–)
Sal	Salinity (Psu)
SEC	Specific energy consumption per unit of desalinated water production (kWh m^{-3})
t	Thickness (m)
T	Temperature (K)
V	Velocity of fluid (m s^{-1})
W	Power output (kW)
W_i	Width (m)
x	Quality (–)
X_{tt}	Lockhart–Martinelli parameter (–)
ΔH	Head loss (m)
ΔT	Temperature difference (K)

Subscripts

a	Actual
atm	Atmospheric pressure
atm-fc	Pressure difference between the atmospheric pressure and the flash chamber
BP	Bending pipeline
C	Condenser
CS	Deep seawater
CSI	Deep seawater inlet
CSO	Deep seawater outlet
CW	Temperature of condenser plate wall
D	Desalination
DW	Desalinated water
DWP	Desalinated water production power
e	Equivalent
E	Eva-con
EW	Temperature of evaporator plate wall
F	Flash point
G	Generator
HX	Heat exchanger
l	Liquid
m	Average
SP	Straight pipeline
T	Turbine
TOTAL	Total heat transfer area of heat exchanger
th	Thermal
v	Vapor
W	Temperature at the plate wall
WF	Working fluid
WFS	Working fluid considering separator
WS	Warm surface seawater
WSI	Warm surface seawater inlet
WSO	Warm surface outlet

Acronyms

BPE	Boiling point elevation
C-OTEC	Closed-cycle ocean thermal energy conversion
H-OTEC	Hybrid-cycle ocean thermal energy conversion
NETD	Non-equilibrium temperature difference
OTEC	Ocean thermal energy conversion

Greek letters

α	Heat transfer coefficient (kW m^{-2} K^{-1})
γ	Objective function (m^2 kW^{-1})
Δ	Difference
η	Efficiency (%)
λ	Thermal conductivity (kW m^{-1} K^{-1})
π	Pi (–)
ρ	Density (kg m^{-3})
μ	Dynamic viscosity (Pa s)
ϕ	Enlargement (–)

1 Introduction

The issue of freshwater scarcity presents a pressing challenge for populations inhabiting archipelagic regions [1]. Remarkably, freshwater constitutes merely 2.5% of Earth's total water volume, with the largest proportion being subterranean [2]. This subterranean water primarily serves as the main resource for these populations, yet its salinity increases with greater depth. Typically, the salinity surpasses 500 mg/L NaCl, rendering the water unfit for consumption as per the guidelines set forth by the World Health Organization (WHO) for potable water [3]. Notably, the task of securing freshwater sources is becoming challenging as development on these islands continues to rise. Therefore, by 2030, the United Nations' Sustainable Development Goal 6 endeavors to realize the aim of providing "*clean water and sanitation for all*" [4].

Researchers have directed their focus towards desalination technologies, recognizing them as pivotal in achieving the specified goal [5, 6]. Desalination, in essence, is a method to remove salt from saline water. Presently, numerous techniques, including multi-stage flash (MSF), multiple-effect distillation (MED), electrodialysis (ED), and reverse osmosis (RO), have been firmly established as effective means to obtain freshwater [7–10]. Unfortunately, these methods are dependent on stable power supply. This is challenging given that a significant number of inhabitants on these islands lack access to conventional power grids and predominantly rely on diesel generators for their energy. Note that current conventional large-scale desalination technologies use fossil fuels as a resource to generate intensive thermal energy or electricity [7]. By 2050, it is anticipated that the annual emissions of carbon equivalents from fossil fuels powered desalination

facilities globally will climb to 400 million tons [8, 9]. This not only contributes to greenhouse gas emissions but also contradicts the global endeavors aimed at mitigating climate change.

In response to this challenge, researchers have explored the possibility of employing renewable energy sources to drive the desalination plant. This approach is favored for its environmentally friendly and enhanced sustainability. While these advantages are crucial, it also holds the capacity to reduce the eventual cost for end-users, which is of vital importance for residents in disadvantaged communities [9]. The ocean, which covers about 70% of Earth's surface, possesses abundant thermal energy, especially in the tropics. This not only represents the most substantial reservoir of thermal energy resources but also delivers consistent energy output [10]. Ocean thermal energy conversion (OTEC) is the application of thermal gradient that generates a clean renewable and always accessible base-load power. Several simulations have also been documented, demonstrating the theoretical capability of OTEC to globally generate annual power output of up to 30 terawatts from a depth of 1000 m [11]. Hence, using OTEC technology to drive desalination process presents a viable approach to achieving environmentally friendly and sustainable freshwater production, particularly in tropical islands.

Open cycle OTEC (O-OTEC) was proposed in 1881 by the famous French physicist Dr. d'Arsonval [12]. Unfortunately, O-OTEC faces challenges primarily attributed to the substantial turbine diameters required as the power generation scale increases, demanding significant initial investment [13]. To address this challenge, a closed-cycle OTEC (C-OTEC) was developed. This involves utilizing a low boiling point working fluid within a loop, with the surface and deep seawater serving as the heat source and sink, respectively. The C-OTEC design permits the utilization of a turbine with a reduced size compared to O-OTEC [14]. However, it is important to note that the C-OTEC design is solely focused on power generation and does not produce water. An alternative approach was proposed by Uehara et al. [15], who suggested integrating C-OTEC with spray flash evaporation to yield some amount of desalinated water. Spray flash evaporation plays a prominent role in the separation and heat transfer aspects of desalination technology, particularly when driven by renewable energy. Ikegami et al. [16] conducted experimental comparisons of the spray flash desalination process, specifically examining downward and upward jet flash evaporation using a nozzle. They reported that upward jet methods exhibited higher efficiency and compactness. Subsequently, Mutair and Ikegami [17] conducted experiments to investigate the influencing factors and effects on the intensity of flash evaporation, providing valuable insights for designing the flash evaporation chamber. Moreover, they employed a small spray flash desalination plant capable of producing 15.2 tons of freshwater per day, catering to the needs of low-populated islands and remote areas [18]. This process has also demonstrated sustainability in freshwater production, achieving a rate of 100 tons per day using the ocean thermal gradient, as shown by the National Institute of Ocean Technology (NIOT) since 2005 [19]. Some researchers, for example Liponi et al. [20] conducted research on coupling C-OTEC with RO for freshwater generation. However, the purity of the brine discharge from flash desalination, tends to be higher than that from RO methods [21]. Moreover, the brine rejected from RO usually contains higher salt content and various compounds that could have adverse effects on marine ecosystems [22]. Nonetheless, the discharge of water from OTEC may still pose environmental challenges. A researcher has developed a model projecting that with the increase in OTEC's MW scale, adverse effects on coral may manifest due to elevated nitrate (NO_3) concentration near the discharge site [23]. Furthermore, the design of C-OTEC encourages the occurrence of biofouling within the heat exchanger. A more recent development is the hybrid cycle OTEC (H-OTEC), which combines elements from both O-OTEC and C-OTEC. This approach introduces additional benefits, including the prevention of biofouling and corrosion in the heat exchanger. As a result, it becomes feasible to employ lower-grade materials the like of stainless steel and aluminum instead of titanium [24]. In 2018, Song [25] conducted research on a 634 kW H-OTEC, resulting in a freshwater production of 55.1 $m^3\ h^{-1}$. The findings exhibited that H-OTEC yields greater desalinated water compared to O-OTEC, with the added advantage of lower capital costs.

In the traditional objective function to assess OTEC plant, by Uehara and Ikegami [26], minimizing the ratio of total heat exchanger area to net power output is examined, with the evaluation focusing solely on net power. This focus on net power stems from the exclusive power generation of the closed OTEC (C-OTEC) design. An analysis of the same objective function was conducted by Bernardoni et al. [27], revealing that heat exchangers constitute a significant portion of expenses within an offshore C-OTEC plant, accounting for approximately 36% of the overall cost. This aligns with the findings of Langer et al. [28], in which heat exchanger expenses were identified as the predominant component at 28%. Adiputra et al. [29] stated that the cost of heat exchanger takes up a significant portion, approximately 21%, of the total cost. A recent investigation by Thirugnana et al. [30] also centered on the identical objective function, examining a 10 MW C-OTEC plant situated in Malaysia. It is important to note that H-OTEC is not intended to be integrated with a desalination system; instead, it operates as an independent facility for water and power generation. In a previous

investigation conducted by Uehara et al. [15], the scope was limited to a comparison between C-OTEC integrated desalination and H-OTEC without integrated desalination. As of today, there have been numerous innovative studies on the comprehensive application of OTEC technology for various multi-generation purposes. For example, Zhou et al. [31] examined the performance of C-OTEC when combined with solar energy, multi-effect desalination, and cooling. Yuan investigated a novel C-OTEC system paired with solar energy for both power generation and cold storage refrigeration [32]. However, the insufficient thermal energy results in the difficulty to drive the ejector refrigeration power cycle and limited water productivity. In the field of OTEC, this shortfall is typically addressed by introducing solar energy as auxiliary heating. Hu et al. [33] recently proposed a distillation desalination system that combines OTEC and solar energy. In this system, OTEC is harnessed to provide a sustainable source of freshwater, while the integration of solar energy serves to increase the heat source temperature and enhance freshwater production. However, it is essential to carefully estimate additional costs, including maintenance expenses for solar panels, which considers specific plumbing, piping, and sealing requirements to prevent damage from saltwater. Failing to do so could potentially compromise the practical feasibility and reliability of an OTEC integrated with solar energy system [34]. However, up until this point, no work has been done regarding the integration of flash desalination into H-OTEC, leaving its operational performance and efficiency largely unexplored.

In the current H-OTEC configuration, the system yields two products: power and desalinated water. Nonetheless, if the objective function proposed by Uehara and Ikegami [26] is used, the desalinated water product remains unaccounted for. Thus, a comprehensive evaluation of H-OTEC necessitates the consideration of both electricity and desalinated water. For commercial-scale megawatt-class power generation using an OTEC system, a substantial amount of seawater is necessary due to the low temperature difference gradient. Since less than 1% of the surface seawater undergoes flash evaporation, a significant portion of the heat from the seawater exiting the flash chamber is wasted [15]. Therefore, supplying the remaining heat to an integrated desalination system is a viable solution to enhance water production rate. Concerning water production rate, the necessary power for water production is calculated. The RO process for seawater desalination has demonstrated one of the most efficient energy consumption profiles in terms of electricity consumption. This energy consumption greatly depends on the membrane characteristics and water quality. By implementing a research finding's by Al Zahrani's [35], the water production flowrate is converted into an equivalent water production power.

In this work, H-OTEC integrated desalination (H-OTEC + D) is proposed which is expected to improve its performance compared to conventional H-OTEC. Rather than increasing costs by adding auxiliary heating source equipment, equivalent water production power is considered to maximize the power and desalinated water production of H-OTEC + D using the proposed objective function. Initially, an optimization process was conducted for both H-OTEC + D and conventional H-OTEC models using the Fortran framework. This optimization was carried out employing both the conventional objective function and proposed objective function. To assess the system's optimization performance, temperature difference (ΔT) was varied and results such as power generation, desalinated water yield, pumping power consumption, surface and deep seawater flow rates, heat transfer area, and desalination ratio are analyzed.

2 Systems description

2.1 H-OTEC + D and H-OTEC

Figures 1 and 2 represent the schematic diagram and the conceptual temperature-entropy (T–s diagram) of H-OTEC + D system, respectively, while Figs. 3 and 4 exhibit the schematic diagram and the conceptual temperature-entropy (T–s diagram) of H-OTEC system, respectively. For the H-OTEC description, the system consists of two parts, namely flash desalination and power generation, the latter being based on the Rankine cycle. The surface seawater is drawn into the system and is flash evaporated under vacuum condition (around 3 kPa) to form steam. Such a process enables the prevention of biofouling as other impurities are restrained from entering the evaporator-condenser (eva-con). The condensation of this steam releases a substantial amount of latent heat which is then transferred to the working fluid side. The desalinated water obtained through steam condensation is then collected in a tank. The working fluid undergoes evaporation, forming a high-pressure vapor, which is directed into separator to ensure that any residual liquid is recycled back to the evaporator. This is to make certain only saturated vapor may enter the turbine inlet. The vapor working fluid expands, generating power in the generator. Then, the exhaust vapor enters the condenser where it is condensed by deep seawater drawn from a depth of over 600 m. The pressure difference between the turbine and condenser enables the turbine and drives the generator. After condensation, the working fluid is pumped back into the evaporator and the cycle continues.

The desalination part of H-OTEC is referred to as 1st-stage desalination, while the desalination plant as the 2nd-stage desalination. The surface seawater outlet from

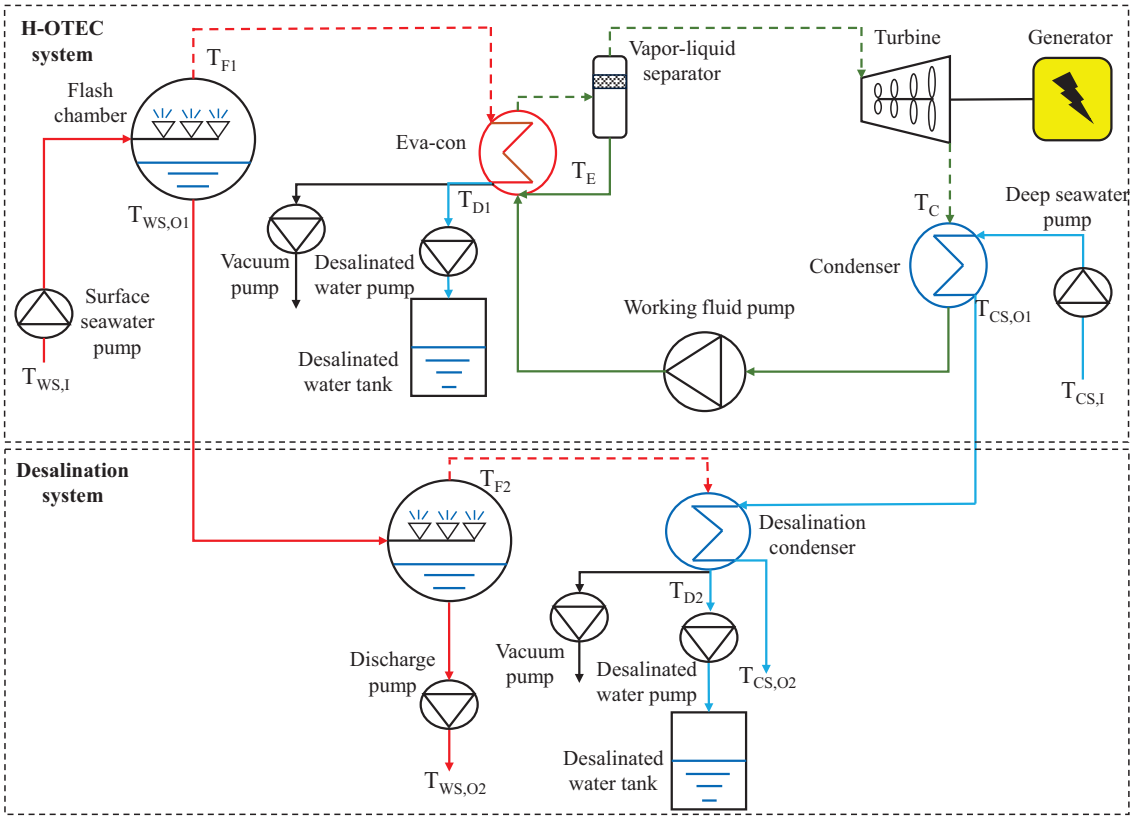

Fig. 1 Schematic diagram of H-OTEC + D system

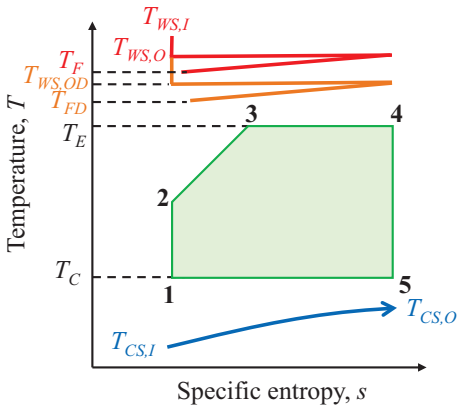

Fig. 2 The conceptual T–s diagram of H-OTEC + D system

1st-stage desalination is directed towards the second flash chamber for flashing. Subsequently, the steam vapor proceeds into the desalination condenser, where it undergoes condensation by the deep seawater passing through the condenser within the H-OTEC system.

The performance of H-OTEC is evaluated under several limitations and assumptions as listed as follows:

- To minimize the dry out area and heat transfer performance reduction, the quality of working fluid at the evaporator outlet is fixed at 0.8 rather than at 1 [36].
- The working fluid is in a saturated vapor state at the turbine inlet.
- The working fluid is in a saturated liquid state at the condenser outlet.
- The heat losses occurring to surrounding is negligible.
- The temperature increase of the deep seawater during the inlet process is not considered.
- The non-condensable gases from the surface can impact the condensation performance within the eva-con. However, in this scenario, it is assumed that a system capable of effectively removing the non-condensable gases is in place [15].
- The flash temperature, T_F, and desalinated water temperature, T_D, are constant due to the process of latent heat of condensation. Although the sensible heat has a non-negligible impact on the temperature change of desalinated water, it is not considered due to the dominant effect of latent heat.

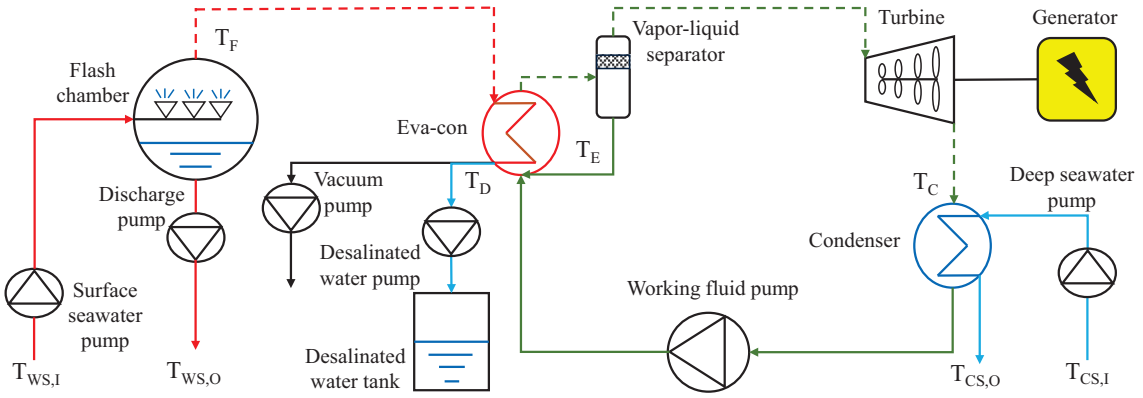

Fig. 3 Schematic diagram of H-OTEC system

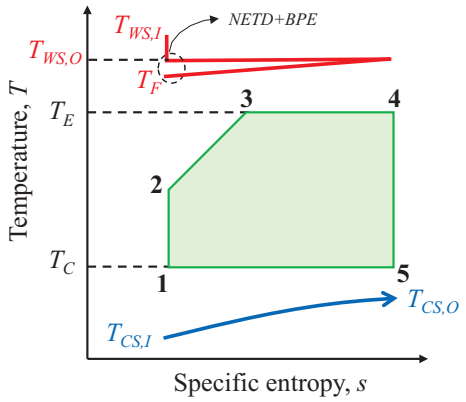

Fig. 4 The conceptual T–s diagram of H-OTEC system

2.2 Objective function

The initial step prior optimization is to establish the objective function that is to be minimized. This present study defines two distinct objective functions to facilitate a comparative analysis between H-OTEC + D and H-OTEC. The following is the conventional objective function, γ_1 which is represented as a ratio between two variables is listed as follows:

$$\gamma_1 = \frac{A_{\mathrm{TOTAL}}}{W_N} \tag{1}$$

$$A_{\mathrm{TOTAL}} = A_{\mathrm{E}} + A_{\mathrm{C}} + A_{\mathrm{DC}} \tag{2}$$

where A_{TOTAL} is the total heat transfer area of heat exchanger, and W is the net power output. The subscript E, C and DC stand for eva-con, condenser and desalination condenser, respectively. It is important to note that the objective function can be defined as the ratio of total power plant cost to the net power per unit. However, this total cost can fluctuate based on factors such as the timing of construction and the design which pose a challenge. Given that the cost of the heat exchanger represents a substantial portion of the OTEC plant's expenses, it is more effective to utilize the objective function as in Eq. (1) in the optimal design process [26].

To incorporate desalinated water production power in the objective function, γ_2 is proposed as shown in Eq. (3). The equivalent desalinated water production power, W_{DWP}, is a viable means to calculate the desalinated water production power as in Eq. (4):

$$\gamma_2 = \frac{A_{\mathrm{TOTAL}}}{W_N + W_{\mathrm{DWP}}} \tag{3}$$

$$W_{\mathrm{DWP}} = m_{\mathrm{DW}} \times \mathrm{SEC} \tag{4}$$

where m and SEC are the mass flow rate and the specific energy consumption per unit of desalinated water production, respectively. Subscript DW stands for desalinated water. SEC is used in RO systems to express the amount of energy utilized for each unit of water produced [37]. The second-order polynomial equation presented in Eq. (5) serves as a valuable tool for assessing the SEC in desalinated water production [38]. This equation takes into account the salinity factor measured in practical salinity unit (PSU), which varies based on geographical locations. Equation (5) data have been extracted and reproduced from a study conducted by Zahrani et al. [35]. It is crucial to emphasize that the referred RO system incorporates contributions from a pump, an RO module, and a hydraulic turbine:

$$\mathrm{SEC} = 0.0003\mathrm{Sal}^2 + 0.0018\mathrm{Sal} + 2.6049 \tag{5}$$

where Sal is the salinity in Psu.

2.3 Power generation and head loss

The net power output of an H-OTEC system relies on the harvested heat from the temperature difference which produces gross power output. For H-OTEC and H-OTEC + D, the W_N is given as in Eq. (6):

$$W_N = W_G - \left(W_{WS} + W_{DW} + W_{CS} + W_{WF} + W_V\right) \tag{6}$$

where W_G is the gross power output, W_{WS} represents the overall pumping power for surface seawater and its discharge, W_{DW} is the discharge pumping power of desalinated water, W_{CS} is the pumping power for deep seawater, and W_{WF} is the pumping power for working fluid. Due to the requirement of vacuum condition inside the flash chamber, W_V which is the vacuum pumping power is necessary. Subscripts WS, CS, and WF, and V stand for surface seawater, deep seawater, working fluid, and vacuum respectively. The W_G and these pumping powers can be written as

$$W_G = m_{WF}\eta_G\eta_T\left(h_4 - h_5\right) \tag{7}$$

$$W_{WS} = \frac{m_{WS}\Delta H_{WS}g}{\eta_{WS}} \tag{8}$$

$$W_{CS} = \frac{m_{CS}\Delta H_{CS}g}{\eta_{CS}} \tag{9}$$

$$W_{WF} = \frac{m_{WF}\Delta H_{WF}g}{\eta_{WF}} \tag{10}$$

$$W_{DW} = \frac{m_{DW}\Delta H_{atm}g}{\eta_D} \tag{11}$$

$$W_V = \frac{W_{AC}}{\eta_V} \tag{12}$$

where ΔH is the total head loss, g is the gravitational acceleration, and η is the pump efficiency. Specifically, to ensure that the flash chamber is in vacuum condition, the adiabatic compression power, W_{AC}, is derived as [15]

$$W_{AC} = \frac{C_a m_{WS} k_a R_a}{2\left(k_a - 1\right)} \left[\left(T_{WSI} + 273.15\right)\left(\left(\frac{30}{17}\right)^{\frac{k_a-1}{k_a}} - 1\right) + \left(T_{sat} + 273.15\right)\left(\left(\frac{P_{atm}}{P_{sat}}\right)^{\frac{k_a-1}{k_a}} - 1\right)\right] \tag{13}$$

where C_a is the mass concentration of air in feed seawater assumed to be 19.36×10^{-6} mg/L. k_a and R_a are the adiabatic compression exponent and specific gas constant of air. P_{atm} and P_{sat} are the atmospheric pressure and saturation pressure of the flash steam.

In addition, the total pressure losses attributed from fluid flow through a system composed of a pipe and heat exchanger are evaluated as

$$\Delta H_{WS} = \Delta H_{SP} + \Delta H_{BP} + \Delta H_{atm-fc} \tag{14}$$

$$\Delta H_{CS} = \Delta H_{SP} + \Delta H_{BP} + \Delta H_{HX} + \Delta H_{\Delta\rho} \tag{15}$$

$$\Delta H_{WF} = \Delta H_{BP} + \Delta H_{WFsat} + \Delta H_{WFeva} + \Delta H_{WFcon} \tag{16}$$

where ΔH_{WS}, ΔH_{CS}, and ΔH_{WF} are the total head loss of pipe for surface seawater, deep seawater, and working fluid, respectively.

Since OTEC operation requires a very long pipe to collect surface and deep seawater, the head loss in the straight pipeline, ΔH_{SP} contributed by the friction can be defined as [39]

$$\Delta H_{SP} = 6.82\frac{Lp}{D^{1.17}}\left(\frac{V_P}{100}\right)^{1.85} \tag{17}$$

$$V_P = \frac{m}{\pi\rho\left(\frac{D}{2}\right)^2} \tag{18}$$

where L_p is the pipe length, D is the diameter of the pipe and V_P is the velocity in the pipe. Note that these equations are applicable to both surface seawater and deep seawater.

The head loss in valves and fittings ΔH_{BP} can be expressed using a modified form of the Darcy–Weisbach equation as [40]

$$\Delta H_{BP} = K\frac{V_P^2}{2g} \tag{19}$$

where K is the resistance coefficient which depends on the selection of elbow used obtained from Ref. [41]. For the surface and deep seawater pipe, the elbow type is assumed to be regular 45° threaded ($K = 0.4$), while working fluid pipe is regular 90° flanged ($K = 0.3$).

Due to the pressure difference inside the flash chamber and the outside atmospheric pressure, repressurization is required to transport away the brine and the desalinated water. Hence, the head loss is denoted as ΔH_{atm}, and can be calculated as follows:

$$\Delta H_{atm-fc} = \frac{P_{atm} - P_F}{\rho_D g} \tag{20}$$

where P_F is the pressure inside the flash chamber.

Since the density of deep seawater exceeds that of surface seawater, it is essential to account for the impact of the pressure differential contributed by the density difference, denoted as $\Delta H_{\Delta\rho}$ as expressed in Ref. [15]:

$$\Delta H_{\Delta\rho} = Lp_{\mathrm{CS}} - \left(\frac{1}{\rho_{\mathrm{CS}}}\right)\left[0.5\left(\rho_{\mathrm{WS}} + \rho_{\mathrm{CS}}\right)L_{\mathrm{CS}}\right] \tag{21}$$

Moreover, the head loss inside the plate heat exchanger ΔH_{HX} is calculated as [26]

$$\Delta H_{\mathrm{HX}} = f\left(\frac{V^2}{2g}\right)\frac{W_i}{d_{\mathrm{e}}} \tag{22}$$

$$d_{\mathrm{e}} = 2 \times C \tag{23}$$

where f is the friction factor. V is the velocity of fluid inside the heat exchanger and W_i is the width of the plate heat exchanger. d_{e} is the equivalent diameter while C is the clearance.

The friction factor of deep seawater in condenser and desalination condenser which is denoted as f_{CS} can be computed as [27]

$$f_{\mathrm{CS}} = \frac{K_{\mathrm{f}}}{\mathrm{Re}^m}, \mathrm{Re} > 300 \tag{24}$$

where Re is the Reynolds number. The values of K_{f} and m, both of which are dependent on a Reynolds number exceeding 300, are considered to be 1.441 and 0.206, respectively [42].

$\Delta H_{\mathrm{WFsat}}$ represents the head loss resulting from the saturation pressure differential that exists between the eva-con and condenser. This equation is taken from Ref. [26]:

$$\Delta H_{\mathrm{WFsat}} = \frac{\left(P_4 - P_1\right)}{\rho_{\mathrm{WF}} g} \tag{25}$$

where P_4 and P_1 are the saturation pressure of the working fluid at the outlet of eva-con and outlet of condenser.

2.4 Heat transfer and mass flow rate

Each number shown in Figs. 2 and 4 represent the state points of the working fluid. The heat transfer rate for the working fluid in eva-con, Q_{E}, can be calculated using the listed equations:

$$Q_{\mathrm{E}} = m_{\mathrm{WF}}\left(h_4 - h_{2\mathrm{a}}\right) \tag{26}$$

$$h_{2\mathrm{a}} = \frac{h_{2\mathrm{s}} - h_1}{\eta_{\mathrm{WF}}} + h_1 \tag{27}$$

where h is the specific enthalpy. Subscripts 4, 2a, and 2s are the position of working fluid at eva-con outlet, actual enthalpy at eva-con inlet, isentropic enthalpy at eva-con inlet, and at condenser outlet, respectively.

The equation Q_{WS} is defined as the heat transfer rate for the surface seawater that flows into the flash chamber of H-OTEC system:

$$Q_{\mathrm{WS}} = m_{\mathrm{WS}} cp_{\mathrm{WS}}\left(T_{\mathrm{WSI}} - T_{\mathrm{WSO}}\right) \tag{28}$$

where T is the temperature and cp is specific heat at constant pressure. Subscripts WSI and WSO are the surface seawater inlet and surface seawater outlet, respectively.

Note that the inlet of eva-con is steam. The surface seawater which has not undergone flash evaporation can be denoted as brine. The calculation of T_{WSO} for H-OTEC can be attained as

$$T_{\mathrm{WSO}} = T_{\mathrm{F}} + \mathrm{NETD} + \mathrm{BPR} \tag{29}$$

$$\mathrm{BPR} = K_{\mathrm{b}} \times \mathrm{molality} \tag{30}$$

$$\mathrm{molality} = \frac{\text{moles of seawater}}{\text{mass of the water}} \tag{31}$$

where the boiling point elevation (BPE) observed in seawater is attributed to the presence of sodium and chlorine ions which elevates the boiling point of seawater. K_{b} is the molal boiling point elevation constant of water which is 0.51 °C kg mol^{-1} [43]. Molality is defined as the number of moles of solute per kilogram of solvent. The standard assumption for the average salinity in the open ocean, 35%, was utilized in this study [44]. Given the number of moles of seawater with 35% salinity in 1000 g of seawater is 0.5996 mol and the mass of water is 0.97728 kg; therefore, the molality can be calculated using Eq. (35). On the other hand, the non-equilibrium temperature difference (NETD) represents the temperature difference between the flash steam and surface seawater inside the flash chamber. The value of NETD is influenced by the size of flash chamber and while it is not being investigated in this study, the value of 0.32 °C was assumed. Since in H-OTEC system, the steam will undergo latent heat of condensation to transfer heat to working fluid, the heat transfer rate, Q_D is computed from the following equation:

$$Q_{\mathrm{D}} = m_{\mathrm{D}} \times L \tag{32}$$

where L is the latent heat.

To obtain the value of latent heat, the equation is obtainable from the following:

$$L = h_{\mathrm{v}} - h_{\mathrm{l}} \tag{33}$$

where the subscript v and l are denotation for the saturated vapor state and saturated liquid state, respectively.

The heat transfer rate for the working fluid in condenser, Q_{C}, is applied:

$$Q_{\mathrm{C}} = m_{\mathrm{WF}}\left(h_{5\mathrm{a}} - h_1\right) \tag{34}$$

$$h_{5\mathrm{a}} = h_4 - \eta_{\mathrm{T}}\left(h_4 - h_{5\mathrm{s}}\right) \tag{35}$$

$$x_5 = \frac{h_{5a} - h_{5l}}{h_{5v} - h_{5l}} \tag{36}$$

where subscript 5a and 5s are the actual specific enthalpy at the condenser inlet and specific enthalpy at condenser outlet, respectively. 5v and 5l are the specific enthalpy at saturated vapor state and saturated liquid state, respectively. x_5 is the quality of the working fluid at condenser inlet while η_T is the turbine efficiency.

For the deep seawater in condenser, Q_{CS} the heat transfer rate equation is defined as follows:

$$Q_{CS} = m_{CS} cp_{CS} \left(T_{CSO} - T_{CSI}\right) \tag{37}$$

where CSO and CSI stand for deep seawater outlet and deep seawater inlet, respectively.

The mass flow rate of the working fluid, surface seawater, desalinated water, and deep seawater can thus be deduced as

$$m_{WF} = \frac{W_T}{h_{5a} - h_4} \tag{38}$$

$$W_T = \frac{W_G}{\eta_G} \tag{39}$$

$$m_{WFS} = \frac{m_{WF}}{x_4} \tag{40}$$

$$m_{WS} = \frac{Q_E}{cp_{WS}\left(T_{WSI} - T_{WSO}\right)} \tag{41}$$

$$m_D = \frac{Q_E}{L} \tag{42}$$

$$m_{CS} = \frac{Q_C}{cp_{CS}\left(T_{CSO} - T_{CSI}\right)} \tag{43}$$

where W_T is the power output of the turbine and η_G is the generator efficiency. m_{WFS} is the mass flow rate of working fluid with separator included in the system, while x_4 is the quality at the turbine inlet.

2.5 Heat balance calculation

The heat balance equations have been carried out for the purpose of validation. The process of heat transfer within the eva-con and condenser is illustrated in Fig. 5. The heat balance calculation is accomplished via a subroutine program, utilizing the bisection method as demonstrated in Fig. 6.

The heat from the flash steam, Q_1, is expressed as

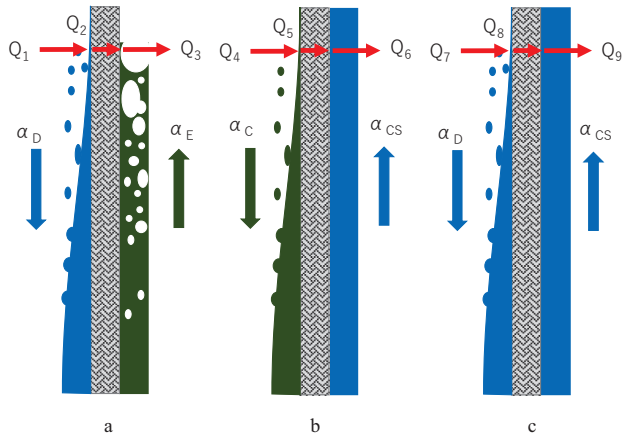

Fig. 5 Heat transfer process inside **a** eva-con, **b** condenser and **c** desalination condenser

$$Q_1 = \alpha A\left(T_D - T_W\right) \tag{44}$$

where α is the heat transfer coefficient, A is the heat transfer area, and T_W is the temperature at the plate wall on seawater side.

Subsequently, thermal energy is transferred within the plate. This equation is applicable to Q_2, Q_5, and Q_8 which can be calculated as shown as follows:

$$Q = \lambda A \frac{\left(T_W - T_{EW}\right)}{t} \tag{45}$$

where λ is the thermal conductivity of the plate and t is the thickness of the plate. T_{EW} is the temperature at the eva-con plate wall on working fluid side.

Finally, the heat transfer to working fluid side is denoted as Q_3, Q_6, and Q_9 which can be computed as

$$Q = \alpha A\left(T_{EW} - T_E\right) \tag{46}$$

where T_E is the evaporation temperature.

However, the direction of heat transfer flow in a condenser is reversed, with thermal energy flowing from the working fluid to the deep seawater. Such process is calculated in the following sequence:

$$Q_{10} = \alpha A\left(T_C - T_{CW}\right) \tag{47}$$

$$Q_{11} = \lambda A \frac{\left(T_{CW} - T_W\right)}{t} \tag{48}$$

$$Q_{12} = \alpha A\left(T_W - \frac{T_{CSI} + T_{CSO}}{2}\right) \tag{49}$$

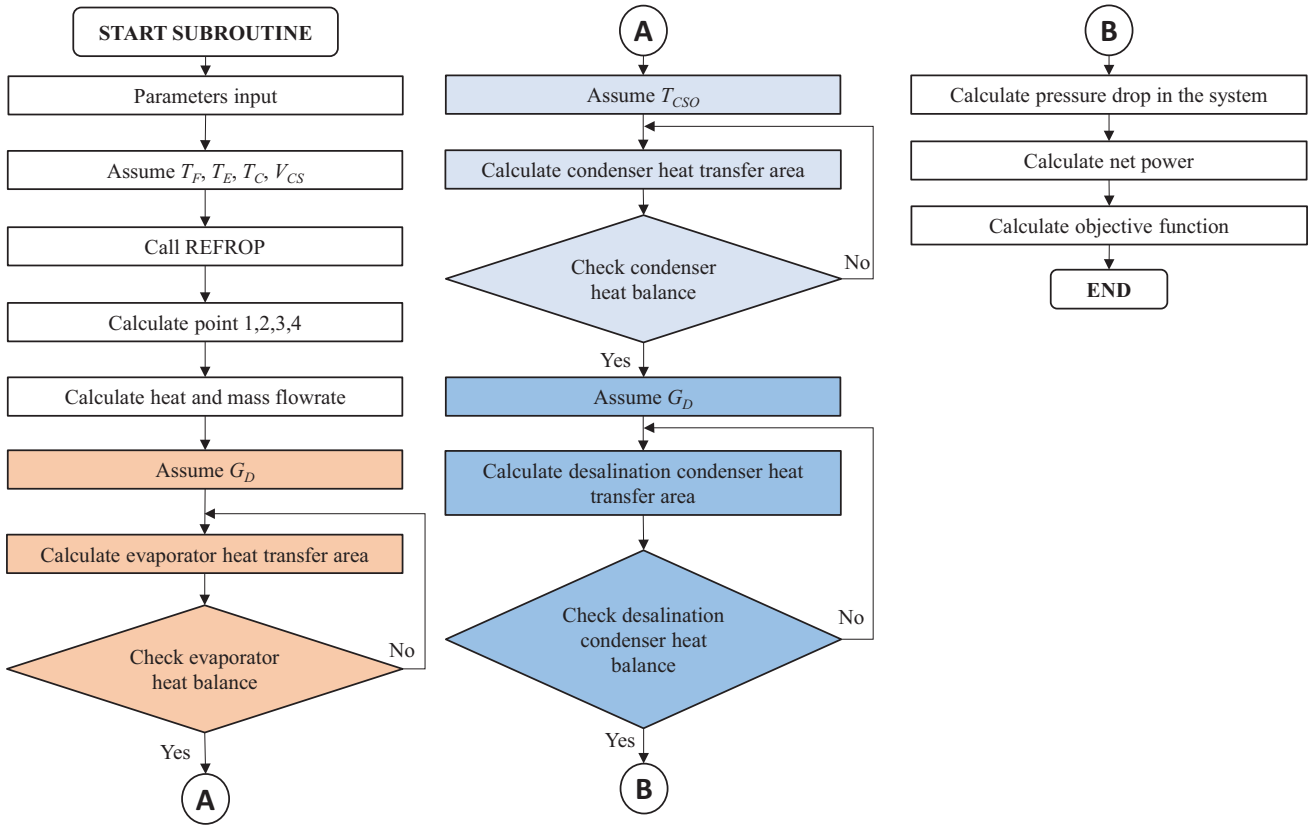

Fig. 6 The flowchart used in this program to calculate the subroutine program using bisection method

where T_C and T_{CW} are the condensation temperature and the temperature at the condenser plate wall on working fluid side.

2.6 Heat exchanger

The optimal design is carried out to establish the number of plates to calculate the required heat transfer area before maximizing the net power output. To achieve this, various parameters are initially established. For instance, Table 1 presents the heat exchanger dimension values used in this study, which are based on the design conditions from a previous study conducted by Uehara et al. [15].

The heat transfer area of condenser is obtained by following the calculation as follows:

$$A_{CSA} = \frac{m}{(\rho \times V)} \tag{50}$$

$$N = 2 \times \left(\frac{A_{CSA}}{H \times C} - 1 \right) \tag{51}$$

$$A_{CSA,WF} = Wi \times C \times \frac{N}{2} \tag{52}$$

$$A = N \times H \times W_i \times \phi \tag{53}$$

where A_{CSA} and $A_{CSA,WF}$ are the cross-sectional area of seawater side and cross-sectional area of working fluid side, respectively. V is the velocity of seawater inside heat exchanger and N is the number of plates. H and ϕ are the height and enlargement factor, respectively.

Regarding the eva-con, it can be demonstrated as follows:

$$A_{CSA,D} = \frac{m_D}{(2 \times G_D)} \tag{54}$$

$$N = 2 \times \left(\frac{A_{CSA,D}}{H \times C} \right) \tag{55}$$

where $A_{CSA,D}$ is the cross-sectional area of desalinated water side and G is the mass flux.

In the eva-con, the boiling heat transfer coefficient of the working fluid, α_E, is expressed as [45]

Table 1 The heat exchanger specifications

Item	Unit	Eva-con	Condenser	Desalination condenser
Type	–	Plate	Plate	Plate
Height, H	m	4	4	4
Width, W_i	m	1.5	1.5	1.5
Clearance, C	m	0.005	0.005	0.005
Thickness, t	m	0.001	0.001	0.001
Enlargement, ϕ	–	1.07	1.07	1.07
Equivalent diameter, d_e	m	0.01	0.01	0.01
Thermal conductivity, λ	W m^{-1} K^{-1}	15 or 17	17	17
Material	–	Stainless steel	Titanium	Titanium

$$\frac{\alpha_{loc}}{\alpha_{LZ}} = 16.4\left(\frac{1}{X_{tt}}\right)^{1.08} \tag{56}$$

$$\alpha_{LZ} = 0.023\frac{k_l}{D_h}\left[\frac{G(1-x)D_h}{\mu_l}\right]^{0.8}\mathrm{Pr}_l^{0.4} \tag{57}$$

$$X_{tt} = \left(\frac{1-x}{x}\right)^{0.9}\left(\frac{\rho_g}{\rho_l}\right)^{0.5}\left(\frac{\mu_l}{\mu_g}\right)^{0.1}, 780 \le \mathrm{Re} \le 3600 \tag{58}$$

where X_{tt} is the Lockhart–Martinelli parameter and μ is the dynamic viscosity.

The friction factor for evaporation of working fluid at the eva-con can be calculated as follows [46]:

$$f_E = 212\mathrm{Re}_{eq}^{-0.51}P_r^{0.53}, \mathrm{Re} \le 2200 \tag{59}$$

The condensation heat transfer coefficient of the desalinated water, α_D, and working fluid, α_C, are expressed as follows [47]:

$$\alpha = 1.875\varnothing\frac{\lambda}{D_{eq}}\mathrm{Re}_{eq}^{0.445}\mathrm{Pr}_l^{1/3} \tag{60}$$

$$\mathrm{Re}_{eq} = \frac{G_{eq}(1-x)D_h}{\mu_l}, \mathrm{Re} < 1600 \text{ and } \mathrm{Re} \ge 1600 \tag{61}$$

$$G_{eq} = G\left[1 - X_m + X_m\left(\frac{\rho_l}{\rho_v}\right)^{1/2}\right] \tag{62}$$

where X_m is the average vapor quality.

The friction factor for condensation of working fluid at condenser can be calculated as shown as follows [48]:

$$f_{LT1} = (1.8\log\mathrm{Re} - 1.5)^{-2}, \mathrm{Re} \ge 2000 \tag{63}$$

$$f_{LT2} = 3.8\left(39\mathrm{Re}^{-0.289}\right), \mathrm{Re} \ge 2000 \tag{64}$$

$$f = \left(\frac{\cos\beta}{\sqrt{0.18\tan\beta + 0.36\sin\beta + f_{LT1}/\cos\beta}} + \frac{1-\cos\beta}{\sqrt{f_{LT2}}}\right)^{-2} \tag{65}$$

For the deep seawater side, the heat transfer coefficient, α_{CS}, is calculated as [49]

$$\alpha = 0.159\frac{\lambda}{D_e}\mathrm{Re}^{0.64}\mathrm{Pr}^{0.4}, 2 \le \mathrm{Re} \le 6000 \tag{66}$$

2.7 Optimization model

The present study details the development of an optimized OTEC model via the programming language Fortran framework. It was realized via the method of steepest descent by finding the minimum value of a given objective function. The simplified flowchart in Fig. 7 was used as the main program, whereby the objective function was expressed as a function of several design parameters which were carefully selected to establish an effective optimization of the H-OTEC model:

$$\gamma = f\left(T_F, T_E, T_C, V_{CS}\right) \tag{67}$$

The simplified graph depicts an iterative optimization process, whereby the objective function is calculated with a fixed set of input design parameters. Subsequently, a new objective function is defined when the value of a design parameter is incrementally changed to minimize the objective function. This updated value of design parameters are then utilized as the initial value for the next design parameter to be optimized and is repeated until the minimum value is attained. Such an iterative process allows for systematic refinement of the design parameters to achieve optimal performance of the system.

H-OTEC system utilizes low boiling working fluid to harness the energy from warm surface and cold deep seawater. Among them, ammonia is widely utilized because

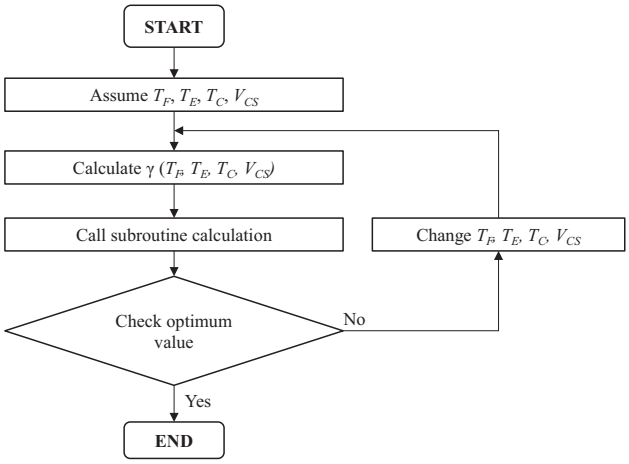

Fig. 7 The simplified flowchart is used in this main program to calculate the minimum value of objective function by means of steepest descent method

the existing temperature difference is sufficient to evaporate. Moreover, its high latent heat and low molar mass properties result in higher particle velocities which lead to smaller pipe sizes [50]. However, ammonia exhibits several negative characteristics, such as its pungent odor, flammability, corrosiveness, and potential explosiveness under specific circumstances. These disadvantages can be offset by the excellent thermodynamic performance. This is further supported by the findings of Wang et al. [49], who reported that ammonia demonstrates the best performance in terms of minimum LCOE and exergy efficiency. All thermophysical properties such as the enthalpy, entropy of each state points are evaluated within the framework of REFROP 10.0 based on the National Institute of Standards and Technology (NIST) database. Furthermore, seawater properties have been replaced with water for the purpose of facilitating the analysis. If seawater were selected, its thermophysical properties would depend on factors such as salinity, dissolved oxygen contents, and non-condensable gases. In this study, we used the salinity factor as an input, as it is an essential component of Eq. (3). Table 2 outlines the specifications required to design H-OTEC + D and H-OTEC.

Table 2 The design conditions for H-OTEC and H-OTEC + D

Item	Unit	Value
Gross power	MW	10
Generator efficiency, η_G	%	96
Surface seawater temperature, T_{WSI}	°C	24, 28, 32
Deep seawater temperature, T_{CSI}	°C	3, 5, 7
Turbine efficiency, η_T	%	80
Warm surface seawater pump efficiency, η_{WS}	%	75
Desalinated water pump efficiency, η_D	%	75
Deep seawater pump efficiency, η_{CS}	%	75
Working fluid pump efficiency, η_{WF}	%	80
Vacuum pump efficiency, η_V	%	75
Pipe length of surface seawater, Lp_{WS}	m	50
Pipe length of deep seawater, Lp_{CS}	m	800
Diameter pipe of surface seawater, D_{WS}	m	5
Diameter pipe of deep seawater, D_{CS}	m	5
Non-equilibrium temperature difference, NETD	°C	0.3
Stainless steel thermal conductivity, λ_{SS}	$Wm^{-1}\ K^{-1}$	15
Titanium thermal conductivity, λ_{Ti}	$Wm^{-1}\ K^{-1}$	17
Salinity, sal	Psu	35

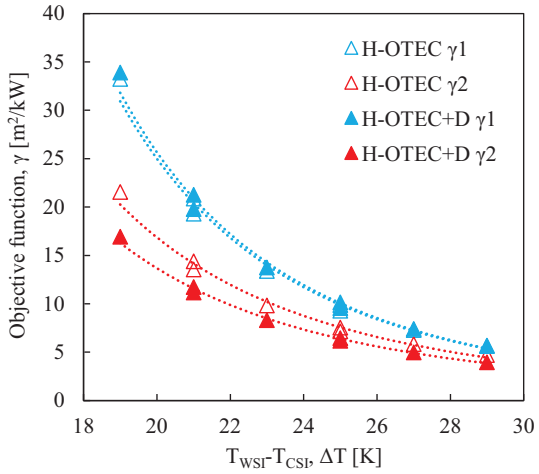

Fig. 8 The comparison involves different objective functions, where γ_1 represents the conventional objective function, and γ_2 is the objective function that considers water production power for H-OTEC and H-OTEC + D

3 Results and discussion

3.1 Objective function

The evaluation in Fig. 8 focuses on the trend of the objective function against ΔT between H-OTEC and H-OTEC + D systems which are both evaluated at γ_1 and γ_2. According to Fig. 8, it shows that the H-OTEC + D γ_2 can be minimized by 33% compared H-OTEC γ_2 at ΔT of 19 °C. By increasing the ΔT, the value of γ_2 for both H-OTEC + D and H-OTEC reduces gradually. When evaluating using γ_1, H-OTEC + D exhibits higher value compared to H-OTEC with a slight difference from 19 until 25 °C. The γ_1 for both systems exhibits almost equivalent value at ΔT greater than 25 °C. This trend demonstrates by accounting both the net power and water production power as the products, the value of γ can be significantly reduced. For instance, evaluating H-OTEC + D at

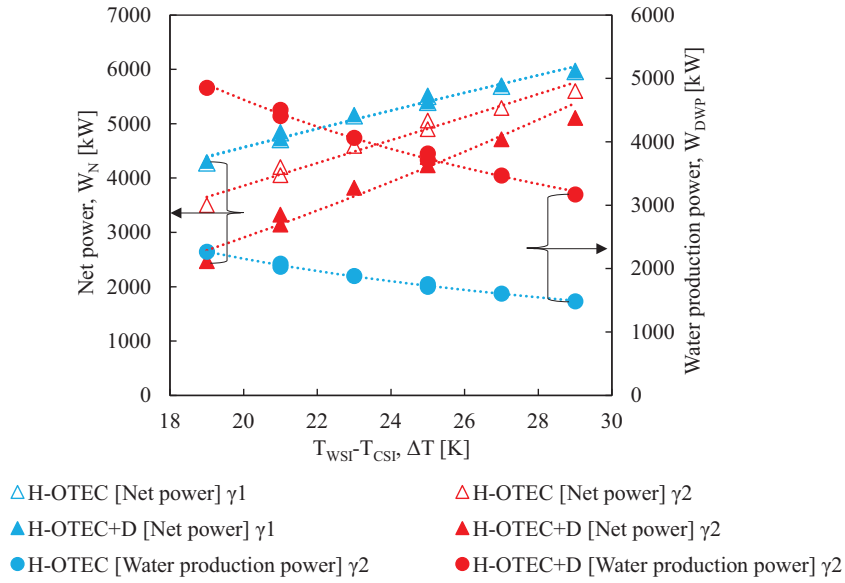

Fig. 9 The relationship between the net power output and water production power for H-OTEC and H-OTEC + D

γ_2 is 53% smaller than H-OTEC + D at γ_1 due to the higher desalinated water production which is calculated in the form of water production power. A similar trend can be observed between H-OTEC γ_2 and H-OTEC γ_1, whereby the former value can be reduced up to 38% at 19 °C. Such percentage gets reduced until 17% as the ΔT increases to 29 °C. Therefore, as the trend shown in Fig. 8, the capital cost of the H-OTEC and H-OTEC + D is smaller when being evaluated using the proposed objective function, γ_2 compared to the conventional objective function, γ_1. In addition, this clearly shows that γ_2 is a more efficient tool to evaluate a H-OTEC and H-OTEC + D, but previous research only introduces net power as the product by following the conventional manner.

3.2 Power generation

Figure 9 represents the relation between the net power output and water production power against ΔT. In the case of net power output, the system evaluated at γ_2 shows a lower value than γ_1. As defined in Eq. (4), the water production power is a function of mass flow rate of desalinated water. Therefore, an optimization with γ_2 maximizes both net power and water production power which resulted in higher flow rate of desalinated water that originates from the higher surface seawater flowrate as shown later in Figs. 11 and 12. The highest net power generation around 5900 kW is by H-OTEC and H-OTEC + D evaluated at γ_1 with temperature difference of 29 °C. It can be observed that the H-OTEC + D γ_1 is slightly lower than H-OTEC γ_1 because of the extra pumping power required to operate the integrated desalination plant. Meanwhile, the net power of H-OTEC γ_2 increases from 34.97 to 56% of the gross power output due to the greater ΔT. However, this percentage of net power at γ_2 decreases to 24.67 and 51% when the desalination plant is powered by the H-OTEC. The integration of water production power indeed reduces the net power significantly, as can be seen from Fig. 9 where the H-OTEC + D barely achieve efficiency greater than 50%, especially at low ΔT. When assessing the water production power, for both H-OTEC and H-OTEC + D opposite trend is noticeable where it decreases as the ΔT increases. Such phenomenon is due to the decreasing intake of surface seawater as more thermal energy is available at higher ΔT. In addition, systems that produce higher net power shows smaller water production power. For instance, at 19 °C, H-OTEC and H-OTEC + D exhibit water production power of 2265 and 4851 kW, respectively. Indeed, it is very crucial to realize that such a trade-off between net power and water production power exists for H-OTEC and H-OTEC + D.

3.3 Desalinated water production

The impact of various objective function affecting the desalinated water production at different ΔT is displayed in Fig. 10. In Fig. 10a which illustrates the total desalinated water production, H-OTEC + D γ_2 displays extremely high yield at 19 °C but this yield experiences a gradual decline as the ΔT increases. This can be attributed to the smaller intake of surface seawater flowrate for the system. The declining trend also can be observed for H-OTEC + D γ_1, H-OTEC γ_1 and H-OTEC γ_2. As can be seen from Fig. 10a, H-OTEC + D regardless γ_1 or γ_2 display higher desalinated water production than standalone H-OTEC at γ_1 or γ_2. This originates from two sources to produce desalinated water: the H-OTEC itself and the integrated desalination plant. When assessed using the proposed objective function, H-OTEC could achieve a maximum increase in water production of

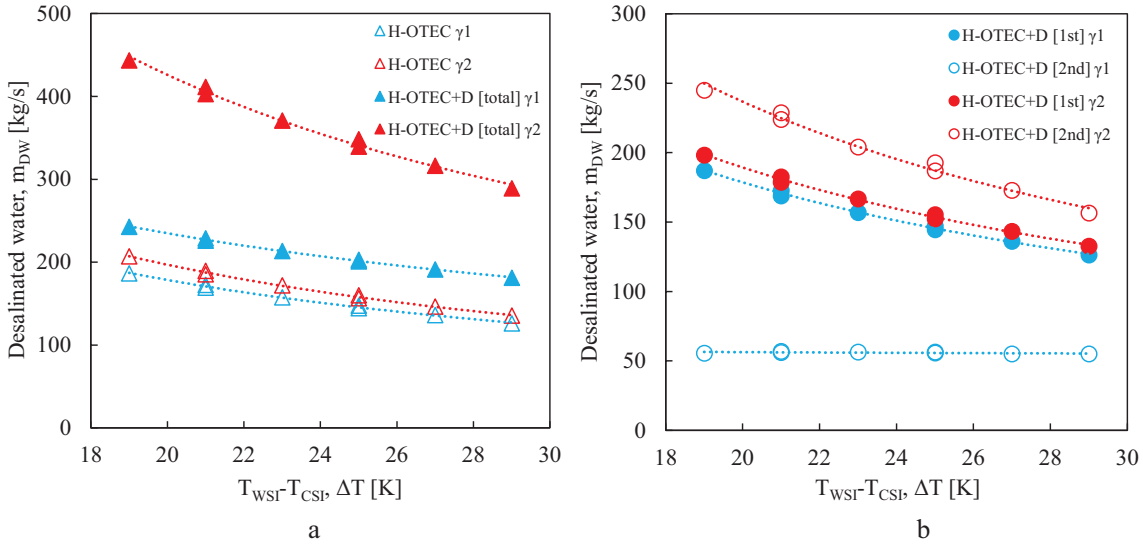

Fig. 10 The effect of different objective functions on desalinated water production where **a** is the total production for H-OTEC and H-OTEC + D, while **b** is the separate production between H-OTEC and the desalination plant

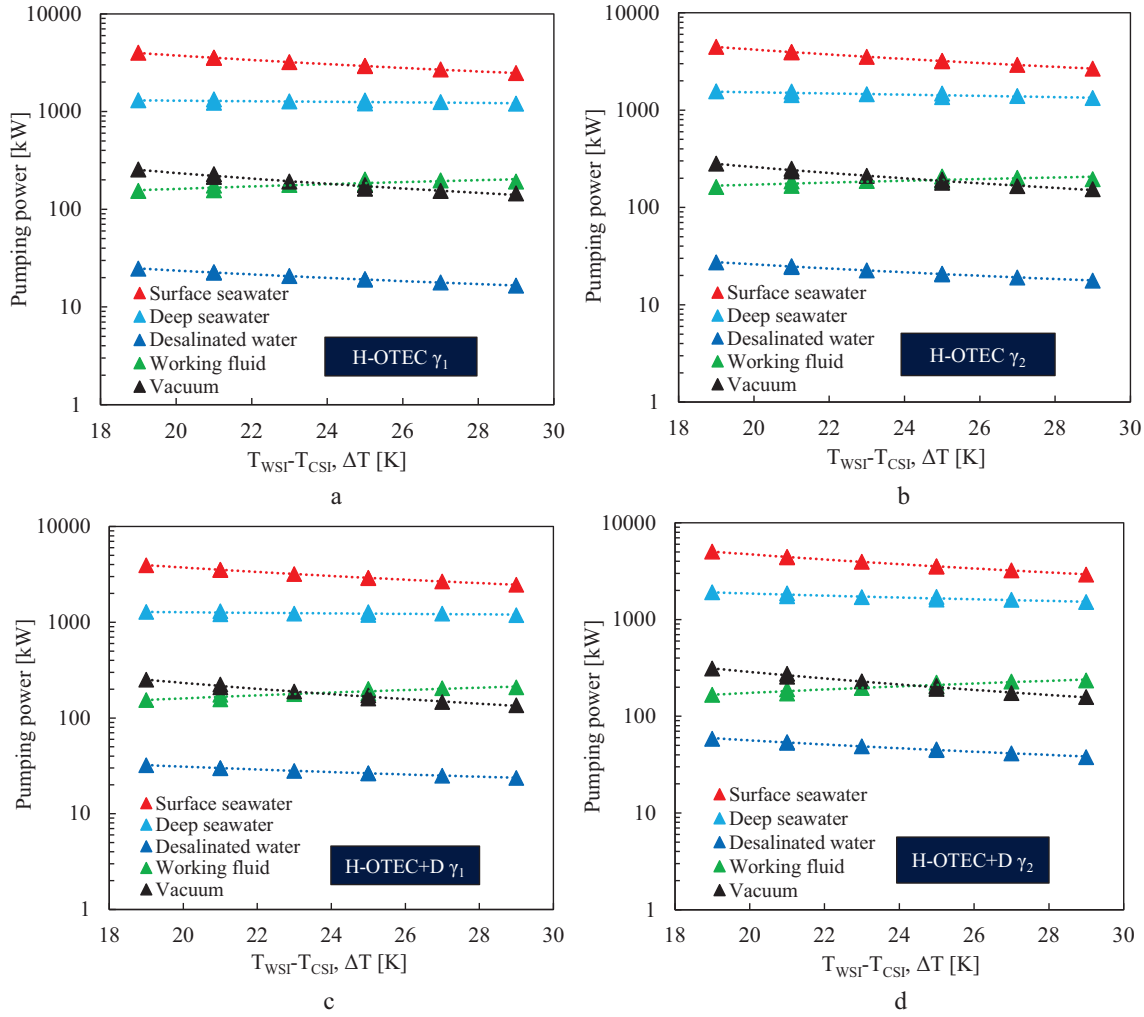

Fig. 11 The breakdown of pumping power consumption for **a** H-OTEC γ_1, **b** H-OTEC γ_2, **c** H-OTEC + D γ_1 and **d** H-OTEC + D γ_2

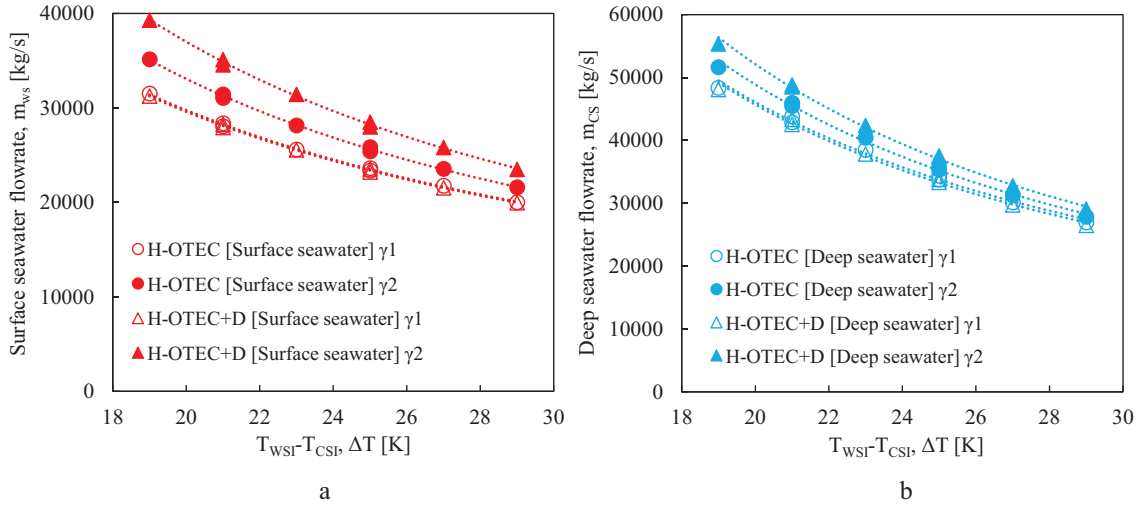

Fig. 12 The effect of temperature difference on the **a** surface and **b** deep seawater flowrate for H-OTEC and H-OTEC + D assessed using γ_1 and γ_2

10% compared to the conventional approach. Furthermore, the role of objective function shows more significant difference when it comes to the output of desalinated water by stages, as illustrated in Fig. 10b. As depicted in the diagram, the term "*1st stage*" refers to the production of desalinated water from the H-OTEC, whereas the term "*2nd stage*" pertains to the output from the integrated desalination plant. For H-OTEC + D γ_1, the 1st stage yields almost similar results as at γ_2; however, the 2nd stage for γ_1 is tremendously low. Since desalinated water is not considered part of the products in γ_1, the system aims to maximize the net power. This necessitates minimizing pumping power, which in turn results in a lower intake flowrate of surface seawater. In contrast to the conventional γ_1, the proposed γ_2 greatly influences the desalinated water production from the 2nd stage. When transitioning the evaluation from γ_1 to γ_2, the 2nd-stage desalinated water production can be augmented by up to 400% at 19 °C, with this percentage gradually decreasing to 220% until 29 °C. Nevertheless, this value remains considerably higher than at γ_1.

3.4 Pumping power consumption

Figure 11 illustrates the distribution of power consumption relative to ΔT, assessed at γ_1 and γ_2 for both H-OTEC and H-OTEC + D. This analysis is significant, as it unveils the precise allocation of power utilized by individual pumping sectors. When examining H-OTEC and H-OTEC + D with different γ, it becomes evident that the proposed γ_2 configuration entails higher pumping power across all sectors. This consequently leads to the notable decrease in net power, as depicted in Fig. 9. Among these scenarios, evaluation using γ_2 requires a greater amount of surface seawater pumping power compared to that at γ_1, as depicted in Fig. 11b, d. Nevertheless, this elevated pumping power results in a higher yield of desalinated water which also leads to a higher desalinated water pumping power. Another factor influencing the greater contribution of surface seawater to the overall pumping power is the substantial power required for discharging, aimed at transporting the brine away from the system. The head loss resulting from the difference between atmospheric pressure and the pressure of the brine is nearly 10 m. In OTEC, given the substantial seawater demand for operations, this leads to a significant surge in pumping power. In terms of the discharge power for desalinated water pumping, although the head loss remains merely at 10 m, the mass flow rate accounts for only 1% of the surface seawater flowrate, resulting in almost negligible pumping power for the overall system. Concerning the vacuum pumping power for all systems, it demonstrates a decreasing trend as the ΔT increases, as it is dependent on the surface seawater as expressed in Eq. (13). In an OTEC system, a higher ΔT signifies a greater potential for heat exchange between the surface seawater and the deep seawater. To capitalize on this increased heat transfer potential, a higher flow rate of ammonia is essential to facilitate increased heat transfer, ensuring the system's efficient operation. Consequently, this leads to a rising trend in the pumping power of the working fluid, correlating with the larger ΔT.

3.5 Surface and deep seawater flowrate

The relationship between surface and deep seawater against ΔT is displayed in Fig. 12. In Fig. 12a, b, each system's surface and deep seawater flowrate show an increased when is evaluated from γ_1 to γ_2. With an

increase in ΔT, there is a corresponding reduction in both surface and deep seawater flowrates. This trend can be elucidated by the fact that a greater amount of thermal energy becomes accessible, resulting in a diminished demand for seawater flowrate. When evaluating using γ_2, the program optimizes for the maximum net power generation and the production of desalinated water. This results in an elevated surface seawater flowrate, consequently leading to an increase in deep seawater flowrate which ensures the efficient absorption of heat supplied by the heat source. The flowrates of both surface and deep seawater are comparable for H-OTEC γ_1 and H-OTEC + D γ_1. However, the latter yields greater desalinated water output as shown in Fig. 9a owing to the incorporation of a second-stage desalination process. Within the H-OTEC system, the flowrate of deep seawater surpasses that of surface seawater. This phenomenon is due to the necessity of applying high discharge pumping power to the surface seawater. Moreover, the optimization program aimed to strike a balance between the flow rates of surface and deep seawater. Excessive surface seawater flow could lead to a detrimental impact on power output. As illustrated in Fig. 11, the surface seawater flowrate contributes the most to the total pumping power due to the high pumping discharge power for the brine. Consequently, an adjustment must be made to the program to manage this excessive pumping power or otherwise, the system could yield a negative net power output.

3.6 Heat transfer area

Figure 13 illustrates a reduction in the total heat transfer area, as well as the heat transfer areas of the eva-con and the condenser, including the desalination condenser, as the value of ΔT increases. In Fig. 13a, for H-OTEC system, it clearly shows that γ_2 could reduce the total heat transfer area by 14% at 19 °C compared to γ_1. However, as the ΔT increases, the total heat transfer area is becoming comparable. This observation indicates that γ_2 serves as an effective tool for reducing the heat exchanger expenses in an H-OTEC plant, concurrently enhancing the output of desalinated water. Interestingly, when the H-OTEC is integrated with a desalination plant and evaluated utilizing γ_2, the overall heat transfer area remains nearly equivalent to that of H-OTEC γ_2, despite the incorporation of a third heat exchanger for the desalination process. This phenomenon can be explained by the substantial reduction in the total heat transfer area for the eva-con and condenser under γ_2, as illustrated in Fig. 13b. As depicted in Fig. 13c, a noticeable contrast is evident between H-OTEC + D at γ_1 and γ_2 concerning the heat transfer area of the desalination condenser. Given the low level of desalinated water production output, as illustrated in Fig. 10b, the desalination plant does not necessitate a substantial heat transfer area for its operation. Hence, these findings emphasize the potential to achieve an H-OTEC + D configuration with nearly identical heat transfer area to that of a standalone H-OTEC system. This adaptation would lead to increased desalinated water production, at the expense of diminished net power output.

3.7 Desalination ratio

Figure 14 exhibits the desalination ratio against ΔT with different objective functions. In this study, the desalination ratio is the function of desalinated water produced per surface seawater flowrate. More specifically, it is a measure of the efficiency of a desalination system in terms of how much fresh water is generated per unit of seawater intake. In Fig. 14a, b, the desalination ratio remains nearly constant as the temperature difference ΔT increases, hovering around 0.6%. Despite the enhanced production of desalinated water observed in H-OTEC at γ_2, the efficiency of the desalination system remains unchanged. When comparing H-OTEC + D at different γ, it is evident that γ_2 shows a higher total desalination ratio of more than 1.2% compared to γ_1 which is less than 1.0%. A notable distinction is in the desalinated water output during the second stage. While γ_1 demonstrates a low desalination ratio, it experiences a 100% increase when evaluated at γ_2, surpassing even the first stage output at γ_2. Such results demonstrate that H-OTEC + D γ_2 is more beneficial since it indicates a more effective use of resources during desalination. Increased ratios can also imply enhanced efficiency of the technology used, resulting in reduced wastage of seawater.

3.8 Conclusion

In time, the dependency of fossil fuels for energy can slowly be replaced by renewable energy. H-OTEC can provide sustainable power generation and freshwater production, particularly in archipelagic regions with an existing ocean temperature gradient. A novel desalination plant driven by renewable energy, such as H-OTEC system, as a new cycle for efficient power and desalinated water production is established and numerically investigated. Its performance is examined and compared with a single H-OTEC setup. Furthermore, a novel objective function is introduced which accounts for both power output and the yield of desalinated water as outputs. Later, a comparison and discussion are carried out regarding the impacts of utilizing conventional and newly proposed objective functions on the H-OTEC and H-OTEC + D systems. The following is a summary of the main conclusions:

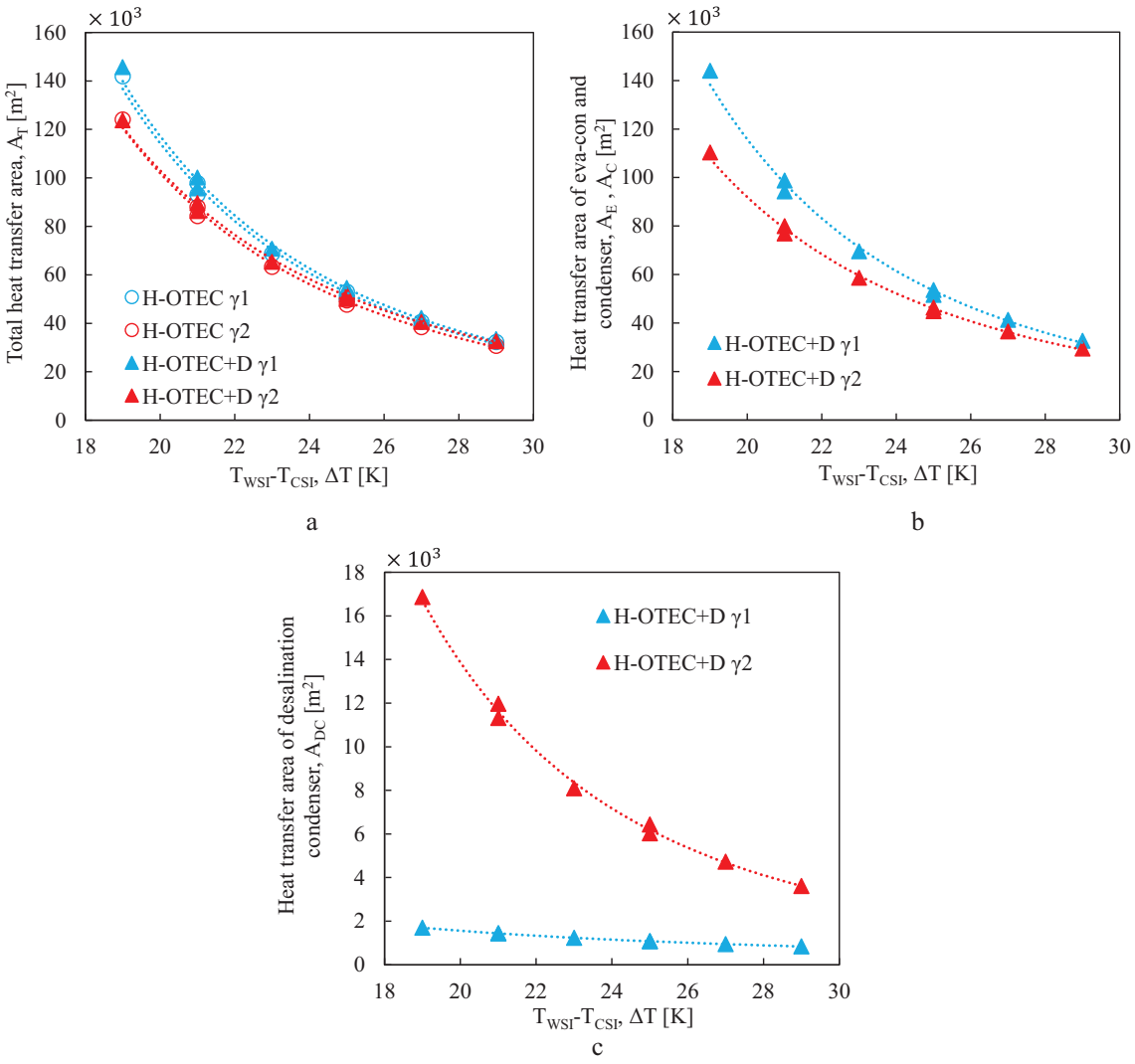

Fig. 13 The heat transfer area evaluated at γ_1 and γ_2, which **a** is the total heat transfer area for all systems. In the H-OTEC + D system, there are two partitions, **b** which is the heat transfer area specific to eva-con and condenser and **c** is the heat transfer area designated for the desalination condenser

(1) The optimization of H-OTEC + D using the proposed objective function has been calculated, demonstrating greater efficiency than H-OTEC alone. The capital cost of H-OTEC + D can be reduced by 33% when evaluated with γ_2 compared to γ_1. Furthermore, the capital cost of H-OTEC + D γ_2 is lower than that of a single H-OTEC γ_2 system. These findings clearly emphasize the enhanced efficiency of γ_2 as an assessment tool for H-OTEC + D.

(2) At the highest ΔT, the net power and desalinated water produced by H-OTEC + D γ_2 is 5100 kW and 289 kg s^{-1}, respectively. While at the lowest ΔT, the net power and desalinated water produced by H-OTEC + D γ_2 is 2467 kW and 443 kg s^{-1}, respectively. It is important to recognize the trade-off between net power and desalinated water production.

(3) The proposed objective function, γ_2 stands out as notably effective in maximizing power generation and desalinated water output while reducing the total heat transfer area, thus resulting in smaller heat exchanger dimensions. In addition, higher desalination ratios for H-OTEC + D can also indicate improved technological efficiency, leading to reduced wastage of seawater.

It is essential to consider the total power, which includes both net power and water production power, when addressing locations with a high demand for fresh water using γ_2. Conversely, in locations where power generation is essential, prioritizing evaluation with γ_1 is recommended. The

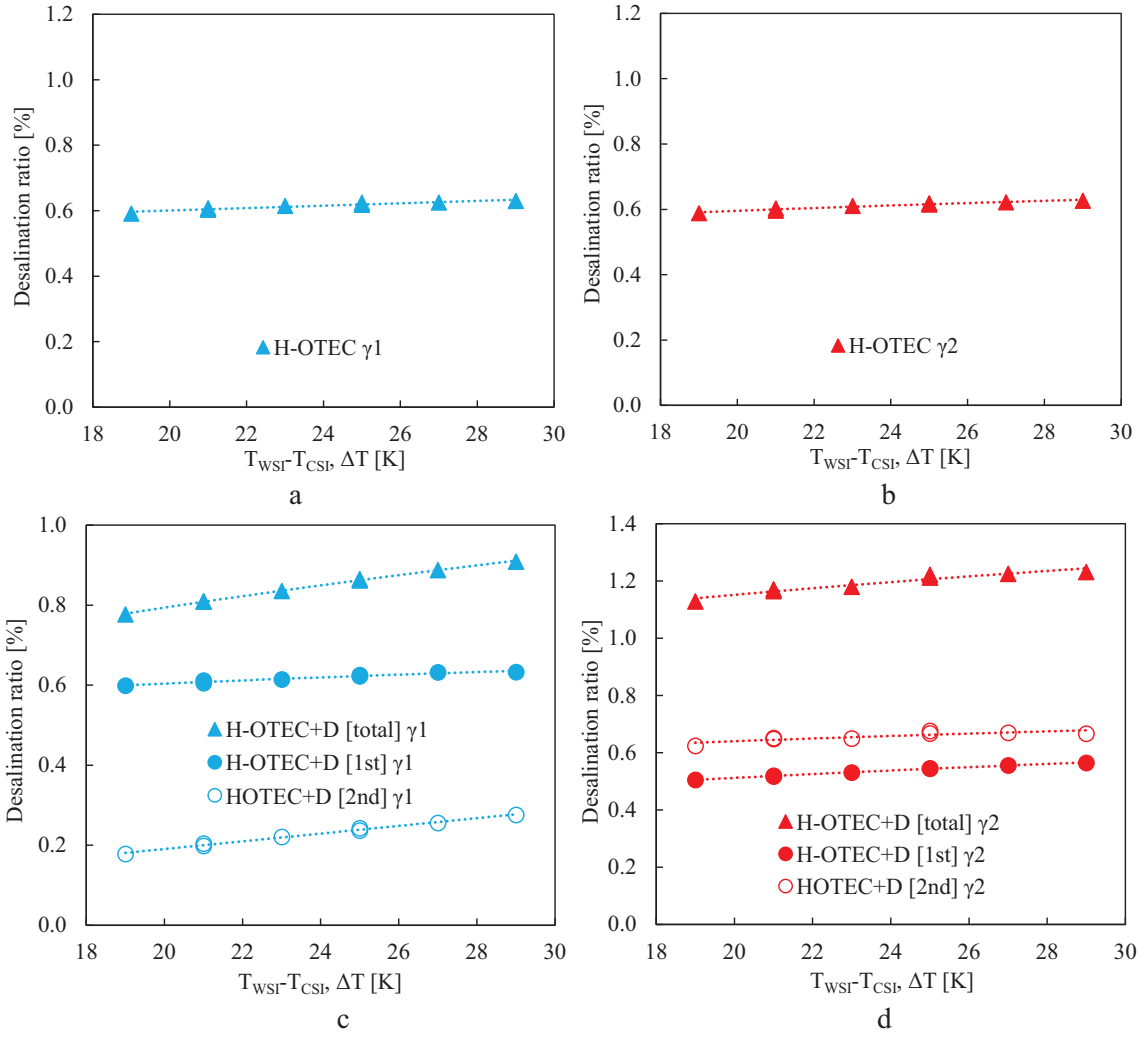

Fig. 14 Desalination ratio with different objective functions which **a** and **b** is for H-OTEC system, while **c** and **d** is for H-OTEC + D

pumping power required repressurization of brine discharge in H-OTEC is significantly high. This is due to the head loss caused by the pressure difference between atmospheric pressure and brine pressure. Given the substantial seawater demand for H-OTEC operations, this leads to a considerable surge in pumping power. Future study will conduct an analysis and evaluation of the H-OTEC system while considering latest flash chamber configuration to overcome the high pumping brine discharge power.

Acknowledgements The authors are grateful for the support provided by the Science and Technology Research Partnership for Sustainable Development (SATREPS), a collaboration between the Japan Science and Technology Agency (JST, JPMJSA1803) and the Japan International Cooperation Agency (JICA), as well as the Ministry of Higher Education (MoHE) of Malaysia for the Long-Term Research Grant Scheme (LRGS) Grant with Vote number R.K130000.7809.4L888 and R.K130000.7856.4L894.

Author contributions AAA: conceptualization, investigation, methodology, review and editing, writing—original draft. TY: conceptualization, review and editing, supervision. KF: conceptualization, methodology. YI: funding acquisition, project administration, review and editing, supervision. TM, TN, STT, ABJ: review and editing, supervision.

Data availability Data and materials will be made available on request.

References

1. Chen Q, Liu Y-Y, Xue C, Yang Y-L, Zhang W-M (2015) Energy self-sufficient desalination stack as a potential fresh water supply on small islands. Desalination 359:52–58
2. Priyantha Ranjan S, Kazama S, Sawamoto M (2006) Effects of climate and land use changes on groundwater resources in coastal aquifers. J Environ Manag 80(1):25–35
3. Organization WH (2004) Guidelines for drinking-water quality. World Health Organization, Geneva
4. Sharma J, Joshi M, Bhatnagar A, Chaurasia AK, Nigam S (2022) Pharmaceutical residues: one of the significant problems in achieving 'clean water for all' and its solution. Environ Res 215:114219
5. Elimelech M, Phillip WA (2011) The future of seawater desalination: energy, technology, and the environment. Science 333(6043):712–717
6. Shannon MA, Bohn PW, Elimelech M, Georgiadis JG, Mariñas BJ, Mayes AM (2008) Science and technology for water purification in the coming decades. Nature 452(7185):301–310
7. Li Z, Siddiqi A, Anadon LD, Narayanamurti V (2018) Towards sustainability in water–energy nexus: ocean energy for seawater desalination. Renew Sustain Energ Rev 82:3833–3847
8. Shahzad MW, Burhan M, Ang L, Ng KC (2017) Energy–water–environment nexus underpinning future desalination sustainability. Desalination 413:52–64
9. Negewo BD (2012) Renewable energy desalination: an emerging solution to close the water gap in the Middle East and North Africa. Mena Development Report
10. Khan N, Kalair A, Abas N, Haider A (2017) Review of ocean tidal, wave and thermal energy technologies. Renew Sustain Energ Rev 72:590–604
11. Rajagopalan K, Nihous GC (2013) Estimates of global Ocean Thermal Energy Conversion (OTEC) resources using an ocean general circulation model. Renew Energy 50:532–540
12. D'Arsonal A (1881) Utilisation de forces naturelles. Revue Scientifique 17:370–372
13. Kim AS, Kim H-J, Lee H-S, Cha S (2016) Dual-use open cycle ocean thermal energy conversion (OC-OTEC) using multiple condensers for adjustable power generation and seawater desalination. Renew Energy 85:344–358
14. Wang T, Ding L, Gu C, Yang B (2008) Performance analysis and improvement for CC-OTEC system. J Mech Sci Technol 22(10):1977–1983
15. Uehara H, Miyara A, Ikegami Y, Nakaoka T (1996) Performance analysis of an OTEC plant and a desalination plant using an integrated hybrid cycle. J Sol Energy Eng 118(2):115–122
16. Ikegami Y, Sasaki H, Gouda T, Uehara H (2006) Experimental study on a spray flash desalination (influence of the direction of injection). Desalination 194(1):81–89
17. Mutair S, Ikegami Y (2009) Experimental study on flash evaporation from superheated water jets: influencing factors and formulation of correlation. Int J Heat Mass Transf 52(23):5643–5651
18. Mutair S, Ikegami Y (2010) Experimental investigation on the characteristics of flash evaporation from superheated water jets for desalination. Desalination 251(1):103–111
19. Sistla PVS, Venkatesan G, Jalihal P, Kathiroli S (2009) low temperature thermal desalination plants. In: Proceedings of the eighth ISOPE ocean mining symposium, Chennai
20. Liponi A, Baccioli A, Vera D, Ferrari L (2022) Seawater desalination through reverse osmosis driven by ocean thermal energy conversion plant: thermodynamic and economic feasibility. Appl Therm Eng 213:118694
21. Guduru S, Bajaj P, Gonsalves ON (2020) India's low temperature thermal desalination technology: water diplomacy with Small Island Developing States in the Indo-Pacific Region. Marit Aff J Nat Mar Found India 16(2):30–45
22. Ali ES, Alsaman AS, Harby K, Askalany AA, Diab MR, Ebrahim Yakoot SM (2017) Recycling brine water of reverse osmosis desalination employing adsorption desalination: a theoretical simulation. Desalination 408:13–24
23. Oshimi R, Tabeta S, Mizuno K (2022) Water quality modeling in subtropical shallow waters to predict environmental impacts of ocean thermal energy conversion. J Mar Sci Technol 27(1):335–347
24. Panchal CB, Bell KJ (1987) Simultaneous production of desalinated water and power using a hybrid-cycle OTEC plant. J Sol Energy Eng 109(2):156–160
25. Song Y (2019) A study of OTEC application on deep-sea FPSOs. J Mar Sci Technol 24(2):466–478
26. Uehara H, Ikegami Y (1990) Optimization of a closed-cycle OTEC system. J Sol Energy Eng 112(4):247–256
27. Bernardoni C, Binotti M, Giostri A (2019) Techno-economic analysis of closed OTEC cycles for power generation. Renew Energy 132:1018–1033
28. Langer J, Quist J, Blok K (2020) Recent progress in the economics of ocean thermal energy conversion: critical review and research agenda. Renew Sustain Energ Rev 130:109960
29. Adiputra R, Utsunomiya T, Koto J, Yasunaga T, Ikegami Y (2020) Preliminary design of a 100 MW-net ocean thermal energy conversion (OTEC) power plant study case: Mentawai island, Indonesia. J Mar Sci Technol 25(1):48–68
30. Thirugnana ST, Jaafar AB, Rajoo S, Azmi AA, Karthikeyan HJ, Yasunaga T, Nakaoka T, Kamyab H, Chelliapan S, Ikegami Y (2023) Performance analysis of a 10 MW ocean thermal energy conversion plant using Rankine Cycle in Malaysia. Sustainability 15(4):3777
31. Zhou S, Liu X, Bian Y, Shen S (2020) Energy, exergy and exergoeconomic analysis of a combined cooling, desalination and power system. Energy Convers Manag 218:113006
32. Yuan H, Zhou P, Mei N (2015) Performance analysis of a solar-assisted OTEC cycle for power generation and fishery cold storage refrigeration. Appl Therm Eng 90:809–819
33. Hu Z, Wang J, Huo E, Zhang C (2023) Investigation of a distillation desalination system driven by solar and ocean thermal energy. Desalination 559:116649
34. Yamada N, Hoshi A, Ikegami Y (2009) Performance simulation of solar-boosted ocean thermal energy conversion plant. Renew Energ 34(7):1752–1758
35. Al-Zahrani A, Orfi J, Al-Suhaibani Z, Salim B, Al-Ansary H (2012) Thermodynamic analysis of a reverse osmosis desalination unit with energy recovery system. Procedia Eng 33:404–414
36. Uehara H, Stuhlträger E, Miyara A, Murakami H, Miyazaki K (1997) Heat transfer and flow resistance of a shell and plate-type evaporator. J Sol Energy Eng 119(2):160–164
37. Tsai SC, Huang WZ, Lin GS, Wang Z, Tung KL, Chuang CJ (2022) Evaluation of the specific energy consumption of sea water reverse osmosis integrated with membrane distillation and pressure-retarded osmosis processes with theoretical models. Membranes 12(4):432
38. Gude GG (2018) Renewable energy powered desalination handbook: application and thermodynamics. Butterworth-Heinemann, Oxford
39. Ikegami Y, Uehara H (1999) Thermodynamic optimization in ocean thermal energy conversion. Thermodyn Optimiz Complex Energy Syst 69:335–344
40. Arnold K, Stewart M (1999) Surface production operations volume 2 design of gas-handling systems and facilities, 2nd edn, pp 343–470
41. Schetz JA, Fuhs AE (1999) Fundamentals of fluid mechanics. Wiley, New York

42. Kakac S, Liu H, Pramuanjaroenkij A (2002) Heat exchangers: selection, rating, and thermal design. CRC Press, Boca Raton
43. Marnoto T, Budiaman IGS, Hapsari CR, Prakosa RAY, Arifin K (2019) Dehydrating ethanol using a ternary solute and extractive batch distillation. MJAS 23(1):124–130
44. Huber C, Klimant I, Krause C, Werner T, Mayr T, Wolfbeis OS (2000) Optical sensor for seawater salinity. Fresenius J Anal Chem 368(2):196–202
45. Arima H, Kim JH, Okamoto A, Ikegami Y (2010) Local boiling heat transfer characteristics of ammonia in a vertical plate evaporator. Int J Refrig 33(2):359–370
46. Khan TS, Khan MS, Chyu M-C, Ayub ZH (2012) Experimental investigation of evaporation heat transfer and pressure drop of ammonia in a 60° chevron plate heat exchanger. Int J Refrig 35(2):336–348
47. Shah MM (2021) Heat transfer during condensation in corrugated plate heat exchangers. Int J Refrig 127:180–193
48. Tao X, Ferreira CAI (2020) NH3 condensation in a plate heat exchanger: flow pattern based models of heat transfer and frictional pressure drop. Int J Heat Mass Transf 154:119774
49. Wang M, Jing R, Zhang H, Meng C, Li N, Zhao Y (2018) An innovative Organic Rankine Cycle (ORC) based Ocean Thermal Energy Conversion (OTEC) system with performance simulation and multi-objective optimization. Appl Therm Eng 145:743–754
50. Armin H (2019) The advantages of natural working fluids. In: Proceedings of the 25th IIR international congress of refrigeration, Montreal